

---

---

# In Vivo Tracking of Th1 Cells by PET Reveals Quantitative and Temporal Distribution and Specific Homing in Lymphatic Tissue

Christoph M. Griessinger<sup>1</sup>, Rainer Kehlbach<sup>2</sup>, Daniel Bukala<sup>1,3</sup>, Stefan Wiehr<sup>1</sup>, Rüdiger Bantleon<sup>2</sup>, Funda Cay<sup>1</sup>, Andreas Schmid<sup>1</sup>, Heidi Braumüller<sup>3</sup>, Birgit Fehrenbacher<sup>3</sup>, Martin Schaller<sup>3</sup>, Martin Eichner<sup>4</sup>, Julie L. Sutcliffe<sup>5</sup>, Walter Ehrlichmann<sup>1</sup>, Oliver Eibl<sup>6</sup>, Gerald Reischl<sup>1</sup>, Simon R. Cherry<sup>5</sup>, Martin Röcken<sup>3</sup>, Bernd J. Pichler<sup>1</sup>, and Manfred Kneilling<sup>1,3</sup>

<sup>1</sup>Department of Preclinical Imaging and Radiopharmacy, Werner Siemens Imaging Center, Eberhard Karls University, Tübingen, Germany; <sup>2</sup>Department of Diagnostic and Interventional Radiology, Eberhard Karls University, Tübingen, Germany; <sup>3</sup>Department of Dermatology, Eberhard Karls University, Tübingen, Germany; <sup>4</sup>Department of Medical Biometry, Eberhard Karls University, Tübingen, Germany; <sup>5</sup>Department of Biomedical Engineering, University of California, Davis, California; and <sup>6</sup>Institute for Applied Physics, Eberhard Karls University, Tübingen, Germany

Although T cells can be labeled for noninvasive in vivo imaging, little is known about the impact of such labeling on T-cell function, and most imaging methods do not provide holistic information about trafficking kinetics, homing sites, or quantification. **Methods:** We developed protocols that minimize the inhibitory effects of <sup>64</sup>Cu-pyruvaldehyde-bis(N4-methylthiosemicarbazone) (<sup>64</sup>Cu-PTSM) labeling on T-cell function and permit the homing patterns of T cells to be followed by PET. Thus, we labeled ovalbumin (OVA) T-cell receptor transgenic interferon (IFN)- $\gamma$ -producing CD4<sup>+</sup> T (Th1) cells with 0.7–2.2 MBq of <sup>64</sup>Cu-PTSM and analyzed cell viability, IFN- $\gamma$  production, proliferation, apoptosis, and DNA double-strand breaks and identified intracellular <sup>64</sup>Cu accumulation sites by energy dispersive x-ray analysis. To elucidate the fate of Th1 cell homing by PET, 10<sup>7</sup> <sup>64</sup>Cu-OVA-Th1 cells were injected intraperitoneally or intravenously into healthy mice. To test the functional capacities of <sup>64</sup>Cu-OVA-Th1 cells during experimental OVA-induced airway hyperreactivity, we injected 10<sup>7</sup> <sup>64</sup>Cu-OVA-Th1 cells intraperitoneally into OVA-immunized or nonimmunized healthy mice, which were challenged with OVA peptide or phosphate-buffered saline or remained untreated. In vivo PET investigations were followed by biodistribution, autoradiography, and fluorescence-activated cell sorting analysis. **Results:** PET revealed unexpected homing patterns depending on the mode of T-cell administration. Within 20 min after intraperitoneal administration, <sup>64</sup>Cu-OVA-Th1 cells homed to the perithymic lymph nodes (LNs) of naive mice. Interestingly, intravenously administered <sup>64</sup>Cu-OVA-Th1 cells homed predominantly into the lung and spleen but not into the perithymic LNs. The accumulation of <sup>64</sup>Cu-OVA-Th1 cells in the pulmonary LNs (6.8  $\pm$  1.1 percentage injected dose per cubic centimeter [%ID/cm<sup>3</sup>]) 24 h after injection was highest in the OVA-immunized and OVA-challenged OVA airway hyperreactivity-diseased littermates 24 h after intraperitoneal administration and lowest in the untreated littermates (3.7  $\pm$  0.4 %ID/cm<sup>3</sup>). As expected, <sup>64</sup>Cu-OVA-Th1 cells also accumulated significantly in the pulmonary LNs of nonimmunized OVA-challenged

animals (6.1  $\pm$  0.5 %ID/cm<sup>3</sup>) when compared with phosphate-buffered saline-challenged animals (4.6  $\pm$  0.5 %ID/cm<sup>3</sup>). **Conclusion:** Our protocol permits the detection of Th1 cells in single LNs and enables temporal in vivo monitoring of T-cell homing over 48 h. This work enables future applications for <sup>64</sup>Cu-PTSM-labeled T cells in clinical trials and novel therapy concepts focusing on T-cell-based immunotherapies of autoimmune diseases or cancer.

**Key Words:** <sup>64</sup>Cu-PTSM; murine Th1 cells; small animal PET; in vivo cell tracking

**J Nucl Med 2014; 55:301–307**  
DOI: 10.2967/jnumed.113.126318

**N**oninvasive in vivo imaging of T-cell trafficking is of prime importance to gain further understanding of the pathogenesis of T-cell-mediated inflammation and to reveal the homing sites, the temporal distribution, and the mode of T-cell action in the context of novel immunotherapies. The use of imaging modalities to follow cell trafficking is also emerging in the fields of regenerative and individualized patient medicine, in which cells of interest must be labeled by appropriate markers to permit their detection in vivo, most likely by optical imaging, ultrasound, PET, or MR imaging. The individual imaging technologies have completely different labeling requirements, and each technique has strengths and weaknesses. For whole-body imaging of cell trafficking, the modalities with the highest potential are PET or MR imaging (1). PET provides exceptional sensitivity in the picomolar range and can reveal dynamic processes with a temporal resolution of several seconds (2). The high sensitivity and approximately 1-mm spatial resolution of the dedicated animal scanner make PET the most appropriate tool to track radiolabeled cells in vivo (3,4). In contrast to PET, MR imaging provides excellent anatomic information but has low sensitivity. For MR imaging, cells can be labeled with superparamagnetic iron oxide particles (SPIOs) that decrease the relaxation times and thus produce negative contrast (5). It is possible to determine the biodistribution of SPIOs-labeled cells in vivo by whole-body MR imaging. However, the sensitivity of MR imaging is approximately 10<sup>6</sup> times

---

Received May 14, 2013; revision accepted Oct. 9, 2013.  
For correspondence or reprints contact: Bernd J. Pichler, Department of Preclinical Imaging and Radiopharmacy, Eberhard Karls University of Tübingen, Röntgenweg 13, 72076 Tübingen, Germany.  
E-mail: Bernd.Pichler@med.uni-tuebingen.de  
Published online Jan. 16, 2014.  
COPYRIGHT © 2014 by the Society of Nuclear Medicine and Molecular Imaging, Inc.

lower than that of PET, limiting its use for the detection of low cell numbers.

The radiolabeling of cells for PET imaging can be achieved by transducing the cells with a reporter gene, such as herpes simplex thymidine kinase, followed by the application of a protein-specific radiolabeled probe, by tagging a radioactive antibody to the cells or by in vitro intracellular labeling with a radiotracer (6–8). All of these methods have distinct benefits and disadvantages. Only a few studies have addressed radioactive T-cell labeling, because this cell population is more prone to be damaged by radiolabeled foreign particles and is more difficult to handle than, for example, cancer or stem cells (9).

Adonai et al. described  $^{64}\text{Cu}$ -pyruvaldehyde-bis(*N*4-methylthiosemicarbazone) ( $^{64}\text{Cu}$ -PTSM) as an intracellular radiolabel for murine lymphocytes (8). The redox-active carrier molecule  $^{64}\text{Cu}$ -PTSM diffuses passively across the cell membrane because of its lipophilicity. Within the cytoplasm, Cu(II)-PTSM is reduced to the unstable Cu(I)-PTSM, resulting in the dissociation of Cu(I) from PTSM. The main step of the cell-labeling process is represented by trapping of the released  $^{64}\text{Cu}$ , which is subsequently bound by intracellular proteins (8,10). Because the positron-emitting radioisotope  $^{64}\text{Cu}$  has a half-life of 12.7 h, noninvasive cell tracking by PET is feasible for a maximum of 2–3 d. Surprisingly, no data exist concerning the impact of  $^{64}\text{Cu}$ -PTSM labeling on the function of lymphocytes.

Here, we evaluated the impact of this label on murine Th1 cells in vitro and in vivo, because Th1 cells enable the visualization of specific homing in the lymph nodes (LNs), the site of MHC-II antigen presentation. We studied the mechanistic properties of the  $^{64}\text{Cu}$ -labeling procedures and developed a  $^{64}\text{Cu}$ -PTSM-labeling protocol with minimized effects on T-cell survival and functions and permitting the monitoring of in vivo T cell trafficking for up to 48 h.

## MATERIALS AND METHODS

### $^{64}\text{Cu}$ -PTSM Ovalbumin (OVA)-Th1 Cell Labeling

To establish an optimized protocol for the  $^{64}\text{Cu}$ -PTSM labeling of mouse Th1 cells,  $1 \times 10^6$  OVA-Th1 cells were incubated for 2, 3, or 4.5 h without or with 0.7, 1.4, or 2.2 MBq of  $^{64}\text{Cu}$ -PTSM in 0.25, 0.5, or 1.0 mL of cell culture medium in 24-well plates at 37°C and 7.5%  $\text{CO}_2$ . For longitudinal in vivo studies, OVA-Th1 cells were always labeled with 0.7 MBq of  $^{64}\text{Cu}$ -PTSM for 3 h. To evaluate the impact of the metal copper and PTSM on the OVA-Th1 cells, we used  $2 \times 10^6$  OVA-Th1 cells in 0.5 mL of cell culture medium (containing 5 U/mL IL-2) in 24-well plates at 37°C and 7.5%  $\text{CO}_2$ . The cells were incubated with 0  $\mu\text{g}$ , 60  $\mu\text{g}$ , or 2  $\mu\text{g}$  of nonradioactive Cu-PTSM or with 0, 0.15, 0.30, or 0.40  $\mu\text{g}$  of PTSM for 2, 3, or 4.5 h. After the incubation, the cells were washed twice and prepared for in vitro and in vivo evaluations.

### In Vivo PET Imaging

Specific OVA-Th1 cell trafficking and homing in mice with OVA-induced airway hyperreactivity (AHR) and untreated control mice were investigated after intraperitoneal (in 200  $\mu\text{L}$  of phosphate-buffered saline [PBS]) or intravenous (in 150  $\mu\text{L}$  of PBS) injection of  $1 \times 10^7$   $^{64}\text{Cu}$ -OVA-Th1 cells, which corresponds to an activity of 0.2–0.5 MBq. The  $^{64}\text{Cu}$ -OVA-Th1 cells were injected immediately after the PET scan was started. The homing of OVA-Th1 cells in untreated BALB/c mice was assessed noninvasively in vivo by PET over 40 h. Dynamic PET scans were obtained over 180 min, and 20-min static PET scans were acquired 3, 7, 16, 27, and 40 h after Th1 cell injection (intravenous or intraperitoneal). Animals with OVA-induced AHR were imaged (static PET scans) 3, 24, and 48 h after Th1 cell injection (intraperitoneal). Mice were anesthetized 10 min before the PET scans

with 1.5% isoflurane in 100% oxygen at a flow rate of 0.7 L/min using a dedicated rodent anesthesia system (Vetland). During the scans, the body temperature of the animals was kept constant at 37°C with a warming pad.

In vivo PET scans were acquired on a small-animal Inveon microPET scanner (Siemens). A 2-dimensional iterative ordered-subset expectation maximization algorithm was used to reconstruct the list mode data. The spatial resolution of the reconstructed PET images was approximately 1.4 mm (3). CT scans were obtained on an Inveon dedicated CT scanner (Siemens). The x-ray voltage was set at 70 keVp, and the current was set to 500  $\mu\text{A}$ . An exposure time of 350 ms and a binning factor of 4 were chosen to yield a reconstructed pixel size of 75  $\mu\text{m}$ . Planar images were acquired from 360 projections over a 360° total rotation in a step-and-shoot mode and reconstructed to obtain a 3-dimensional image. To enable the coregistration of the PET and CT images, we filled glass capillaries with  $^{64}\text{Cu}$ -PTSM and fixed them underneath the mouse bed for use in both scanners.

More methods are provided in the supplemental materials (available at <http://jnm.snmjournals.org>).

## RESULTS

### Specific T-Cell Function After $^{64}\text{Cu}$ -PTSM Labeling

$^{64}\text{Cu}$ -PTSM-radiolabeling protocols were optimized to minimize the impact on Th1 cell function (Fig. 1). OVA-Th1 cells were incubated with 0.7, 1.5, or 2.2 MBq for 2, 3, or 4.5 h, respectively. The radiolabel uptake efficiency and labeling stability were investigated to yield an optimized procedure that consisted of a 3-h incubation of  $10^6$  OVA-Th1 cells with 0.7 MBq of  $^{64}\text{Cu}$ -PTSM in 500  $\mu\text{L}$  of medium (Supplemental Fig. 1A). This labeling protocol permits an acceptable labeling efficiency of 6.5%–9%

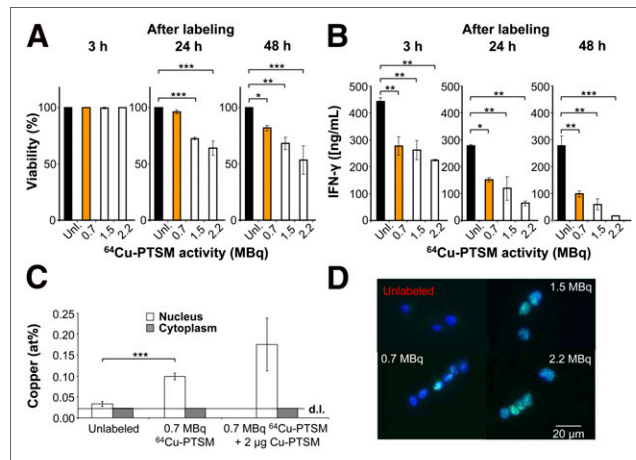


**FIGURE 1.** Impact of  $^{64}\text{Cu}$ -PTSM labeling on viability, T-cell function, and double-strand breaks. (A) Viability after labeling with  $^{64}\text{Cu}$ -PTSM; Dunnett's test. \* $P < 0.05$ . \*\* $P < 0.01$ . \*\*\* $P < 0.001$ . Mean  $\pm$  SD;  $n = 3$ ; 5 independent experiments. (B) IFN- $\gamma$  concentration (ng/mL) in supernatants of OVA-Th1 cells that were cultured for 24 h with irradiated antigen-presenting cells and OVA peptide after labeling with  $^{64}\text{Cu}$ -PTSM; Dunnett's test. \* $P < 0.05$ . \*\* $P < 0.01$ . \*\*\* $P < 0.001$ . Mean  $\pm$  SD;  $n = 2$ ; 3 independent experiments. (C) Mole fraction of copper (mean at percentage  $\pm$  SD) after EDX analysis within nucleus and cytoplasm of OVA-Th1 cells that were unlabeled, labeled with 0.7 MBq of  $^{64}\text{Cu}$ -PTSM, or with 0.7 MBq of  $^{64}\text{Cu}$ -PTSM and 2  $\mu\text{g}$  of Cu-PTSM. Copper mole fraction in cytoplasm was close to detection limit (d.l.) of 0.02 at percentage; 2-sampled Student  $t$  test. \*\*\* $P < 0.001$ . (D) Fluorescence microscopy indicates phosphorylated  $\gamma$ -H2AX in OVA-Th1 cells 3 h after labeling with  $^{64}\text{Cu}$ -PTSM ( $n = 2$ –3) in T-cell nucleus. Green =  $\gamma$ -H2AX antibody; blue = 4', 6-diamidin-2-phenylindol for nuclear staining.

(Supplemental Figs. 1A and 1B). Efflux studies revealed that 47% of  $^{64}\text{Cu}$ -PTSM remained in the OVA-Th1 cells after 5 h and 14% after 24 h, respectively (Supplemental Fig. 1B).

Following this labeling protocol, trypan blue exclusion demonstrated the unaltered viability of Th1 cells 3 h after labeling with 0.7 MBq of  $^{64}\text{Cu}$ -PTSM and only a slight reduction in viability after 24 and 48 h, as compared with the unlabeled control cells (Fig. 1A). Similarly, controls with high concentrations of non-radioactive Cu-PTSM did not show impaired OVA-Th1 cell viability (Supplemental Fig. 1C). A significantly reduced viability was observed when cells were incubated with 1.5 or 2.2 MBq of  $^{64}\text{Cu}$ -PTSM (Fig. 1A). Thus, 3 h of labeling of OVA-Th1 cells with 0.7 MBq of  $^{64}\text{Cu}$ -PTSM appears to be optimal with respect to viability and labeling efficiency.

With regard to specific Th1 cell functions, we observed reduced interferon (IFN)- $\gamma$  concentrations in the supernatants of OVA-Th1 cells labeled with 0.7 MBq of  $^{64}\text{Cu}$ -PTSM at 3, 24, and 48 h after specific stimulation with antigen-presenting cells and OVA peptide when compared with unlabeled OVA-Th1 cells (Fig. 1B). Increased incubation times further reduced the amount of IFN- $\gamma$  in the supernatants (Supplemental Fig. 2A). PTSM alone did not impair the OVA-specific IFN- $\gamma$  secretion of OVA-Th1 cells (Supplemental Fig. 2B), whereas high concentrations of nonradioactive Cu-PTSM strongly suppressed IFN- $\gamma$  secretion (Supplemental Fig. 2C).

The OVA-specific proliferation rate of 0.7 MBq of  $^{64}\text{Cu}$ -PTSM-labeled OVA-Th1 cells, as measured using a  $^3\text{H}$ -thymidine proliferation assay, indicated a 69% reduction in proliferation 3 h after labeling. Interestingly, incubation with a 70-fold-higher concentration of nonradioactive copper reduced OVA-specific Th1 cell proliferation by 35%, which indicates that the metal itself impaired the proliferation (Supplemental Fig. 2D). However, real-time polymerase chain reaction investigations revealed 3 h after labeling normal IFN- $\gamma$  messenger RNA levels and 24 h after labeling enhanced IFN- $\gamma$  messenger RNA levels in  $^{64}\text{Cu}$ -OVA-Th1 cells (Supplemental Fig. 3).

#### Intracellular Localization of $^{64}\text{Cu}$ and DNA Damage

To determine how  $^{64}\text{Cu}$  labeling affects OVA-Th1 cell function, we investigated the intracellular concentration and localization of copper in nonlabeled cells and in cells labeled with 0.7 MBq of  $^{64}\text{Cu}$ -PTSM or with 0.7 MBq of  $^{64}\text{Cu}$ -PTSM plus a 70-fold-higher concentration of nonradioactive Cu-PTSM using electron microscopy and quantitative energy dispersive x-ray (EDX) spectroscopy (Supplemental Fig. 4) (11,12).

Surprisingly,  $^{64}\text{Cu}$  was mainly trapped in the cell nucleus, because the copper mole fraction in the nuclei ( $0.1 \pm 0.01$  at %) of OVA-Th1 cells exposed to 0.7 MBq of  $^{64}\text{Cu}$ -PTSM was higher than that in the cytoplasm. The copper mole fraction of the cytoplasm was close to the detection limit of 0.02%. The copper mole fraction in the nuclei of OVA-Th1 cells labeled with 0.7 MBq of  $^{64}\text{Cu}$ -PTSM was 3.3-fold higher than that in the nuclei of unlabeled cells. Importantly, the investigated cells provided similar  $^{64}\text{Cu}$  concentrations (Fig. 1C).

We assessed phosphorylated histones of the H2AX family ( $\gamma$ -H2AX) by fluorescence microscopy and fluorescence-activated cell sorting (FACS) to investigate whether  $^{64}\text{Cu}$  accumulation within the nuclei leads to radiation-induced DNA double-strand breaks. Fluorescence microscopy analysis of  $\gamma$ -H2AX expression demonstrated double-strand breaks in the nuclei of  $^{64}\text{Cu}$ -PTSM-labeled OVA-Th1 cells (Fig. 1D). The relative  $\gamma$ -H2AX expression 3 h after labeling with 0.7 MBq of  $^{64}\text{Cu}$ -PTSM was approximately

9-fold higher than that of unlabeled OVA-Th1 cells (Supplemental Fig. 5; Supplemental Table 1).

#### In Vivo Homing Patterns After Different Administration Routes of $^{64}\text{Cu}$ -OVA-Th1 Cells

The homing of  $^{64}\text{Cu}$ -PTSM-labeled OVA-Th1 cells was tracked in vivo by PET and fused with CT images to obtain additional anatomic information. We first analyzed the differences in T-cell homing kinetics and biodistribution after intraperitoneal and intravenous administration of  $^{64}\text{Cu}$ -PTSM-labeled OVA-Th1 cells (Fig. 2). Naïve mice were injected intraperitoneally or intravenously with  $10^7$  viable  $^{64}\text{Cu}$ -OVA-Th1 cells, and 180-min dynamic PET scans were obtained immediately after administration. In addition, 20-min static PET data were acquired 3, 7, 16, 27, and 40 h after  $^{64}\text{Cu}$ -OVA-Th1 cell administration (Fig. 2A).

Interestingly, intraperitoneally injected OVA-Th1 cells homed to the perithymic LNs within the first 20 min after administration (Figs. 2A and 2B). Given that  $10^7$  viable  $^{64}\text{Cu}$ -OVA-Th1 cells were injected and neglecting the  $^{64}\text{Cu}$  efflux from the OVA-Th1 cells (Supplemental Fig. 1B), it was possible to detect approxi-

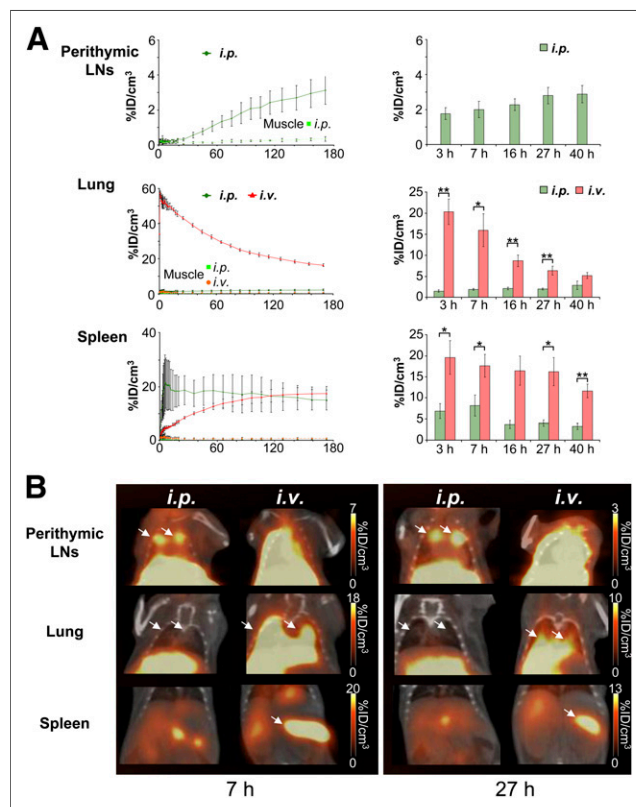


**FIGURE 2.** Different administration routes of  $^{64}\text{Cu}$ -PTSM-labeled OVA-Th1 cells resulted in distinct homing patterns. (A) Time-activity curves ( $\% \text{ID}/\text{cm}^3$ ) derived from perithymic LNs, lung, and spleen after intraperitoneal and intravenous transfer of  $10^7$   $^{64}\text{Cu}$ -PTSM-labeled OVA-Th1 cells display dynamics of OVA-Th1 cell homing in vivo within first 180 min (left; dynamic PET measurement); mean  $\pm$  SEM ( $n = 3$ ). Differences in homing patterns of  $^{64}\text{Cu}$ -OVA-Th1 cells ( $\% \text{ID}/\text{cm}^3$ ) in perithymic LNs, lung, and spleen at 3, 7, 16, 27, and 40 h after intraperitoneal or intravenous administration (static 20-min PET measurements) are shown on right; 2-sampled Student  $t$  test. \* $P < 0.05$ . \*\* $P < 0.01$ . Mean  $\pm$  SEM ( $n = 6$ ). (B) Representative PET/CT images at 7 h (left) and 27 h (right), with focus on perithymic LNs, lung, and spleen (indicated by arrows). i.p. = intraperitoneal; i.v. = intravenous.

mately 60,000  $^{64}\text{Cu}$ -OVA-Th1 cells in 1 individual LN 20 min after intraperitoneal administration ( $0.33 \pm 0.02$  percentage injected dose per cubic centimeter [ $\%ID/\text{cm}^3$ ]). The activity of  $^{64}\text{Cu}$ -OVA-Th1 cells in the perithymic LNs remained constant between  $2.0 \pm 0.5 \%ID/\text{cm}^3$  at 7 h and  $2.9 \pm 0.5 \%ID/\text{cm}^3$  at 40 h after intraperitoneal T-cell transfer. It was not possible to detect specific signals related to  $^{64}\text{Cu}$ -OVA-Th1 cells in the perithymic LNs after intravenous administration because the analysis was impaired by the transient adherence of a high number of  $^{64}\text{Cu}$ -OVA-Th1 cells in the lung, which produced a high background signal.

Thus, in line with the observations in other cell-trafficking studies (8,13,14), many  $^{64}\text{Cu}$ -OVA-Th1 cells nonspecifically accumulated in the lung tissue immediately after intravenous administration ( $57.4 \pm 1.3 \%ID/\text{cm}^3$ ). The signal decreased at a constant rate within the first 180 min to  $16.3 \pm 0.8 \%ID/\text{cm}^3$  and then further to  $5.2 \pm 0.7 \%ID/\text{cm}^3$  at 40 h. In sharp contrast to the intravenous injection, the lung tissue exhibited only background levels of Th1 cell accumulation after intraperitoneal injection (Figs. 2A and 2B).

Within 5 min of intraperitoneal injection,  $^{64}\text{Cu}$ -OVA-Th1 cells accumulated rapidly in the spleen ( $21.1 \pm 6.0 \%ID/\text{cm}^3$ ) and decreased to  $14.8 \pm 2.1 \%ID/\text{cm}^3$  by the end of the 180-min dynamic PET scan. Static PET scans revealed values of  $6.7 \pm 1.8 \%ID/\text{cm}^3$  in the spleen at 3 h and  $3.2 \pm 0.7 \%ID/\text{cm}^3$  at 40 h (Figs. 2A and 2B). The increased values in the spleen in the dynamic PET measurement could be the consequence of an increased spill-over caused by the intraperitoneally injected  $^{64}\text{Cu}$ -OVA-Th1 cells in the peritoneum, intestine, and peripancreatic lymphatic tissue. Mice that underwent dynamic PET scans were anesthetized with 1.5% isoflurane for 3 h, which can cause a reduced intestine movement and motility, yielding a higher accumulation of the  $^{64}\text{Cu}$ -OVA-Th1 cells within the intestines (Supplemental Fig. 6) (15). In contrast, animals that were used for the static PET scans were conscious during the first 3 h. Isoflurane anesthesia evolves well-described antiinflammatory effects applicable to suppress cell migration, further explaining why more of the intraperitoneally injected  $^{64}\text{Cu}$ -OVA-Th1 cells remained in the peritoneal cavity (16).

In contrast, intravenous injection produced a constant increase in the activity accumulation of  $^{64}\text{Cu}$ -OVA-Th1 cells to  $19.4 \pm 4.0 \%ID/\text{cm}^3$  during the 180-min dynamic PET scan. Thereafter, activity of  $^{64}\text{Cu}$ -OVA-Th1 cells decreased in the spleen until 40 h after intravenous injection to  $11.5 \pm 1.7 \%ID/\text{cm}^3$ . Thus, 16–40 h after intravenous administration approximately 3.5-fold more

$^{64}\text{Cu}$ -OVA-Th1 cells homed to the spleen when compared with intraperitoneally injected  $^{64}\text{Cu}$ -OVA-Th1 cells.

Because PET measurements of the intravenously administered  $^{64}\text{Cu}$ -OVA-Th1 cells did not permit the investigation of cell homing to the perithymic LNs, animals were sacrificed 24 h after the intraperitoneal or intravenous administration of  $^{64}\text{Cu}$ -OVA-Th1 cells, the thymus with perithymic LNs was dissected, and autoradiography and hematoxylin and eosin staining of the corresponding tissue sections was performed (Fig. 3). The perithymic LNs were confirmed to be the site of  $^{64}\text{Cu}$ -OVA-Th1 cell accumulation 24 h after intraperitoneal injection; almost no OVA-Th1 cells homed to the perithymic LNs after intravenous administration (Fig. 3A). Additionally ex vivo biodistribution was performed by  $\gamma$  counting of dissected tissue 40 h after intraperitoneal or intravenous administration of  $^{64}\text{Cu}$ -OVA-Th1 cells (Fig. 3B).

To further analyze the homing of intraperitoneally administered OVA-Th1 cells to the perithymic LNs and spleen and the impact of the  $^{64}\text{Cu}$  radiolabel on OVA-Th1 cell homing, we subsequently intraperitoneally injected  $10^7$  nonlabeled or  $^{64}\text{Cu}$ -labeled OVA-Th1 cells into BALB/c mice and performed in vivo PET measurements. The animals were sacrificed after 21 h, the perithymic LNs and spleens were dissected, the lymphocytes were quantified, and FACS analysis was performed to quantify the adoptively transferred OVA-Th1 cells using T-cell receptor-specific antibodies (Fig. 3C; Supplemental Fig. 7). As expected, even without antigen application, intraperitoneally administered OVA-Th1 cells were clearly detected in the perithymic LNs and the spleen. The number of OVA-Th1 cells in the LNs corresponded to previous data published by Schipf et al. (17). No significant differences in the absolute numbers of nonlabeled ( $1.6 \times 10^6 \pm 6.7 \times 10^5$ ) and  $^{64}\text{Cu}$ -OVA-Th1 cells ( $1.8 \times 10^6 \pm 3.1 \times 10^5$ ) were found in the perithymic LNs. Slight increased numbers of  $^{64}\text{Cu}$ -OVA-Th1 cells ( $3.8 \times 10^6 \pm 5.6 \times 10^5$ ), compared with nonlabeled cells ( $2.3 \times 10^6 \pm 2.4 \times 10^5$ ; Fig. 3C), were detected in the spleen. Thus,  $^{64}\text{Cu}$ -PTSM labeling did not affect OVA-Th1 cell-homing properties in vivo.

### Specific Homing of $^{64}\text{Cu}$ -OVA-Th1 Cells in OVA-Induced AHR

To investigate the functional capacities of  $^{64}\text{Cu}$ -OVA-Th1 cells, we tested their ability to home to OVA-specific sites of inflammation using an in vivo model of experimental OVA-induced AHR of the lung (Fig. 4). To determine specific homing, we injected  $10^7$   $^{64}\text{Cu}$ -OVA-Th1 cells intraperitoneally into OVA-immunized or nonimmunized healthy mice. The mice were challenged twice intranasally with OVA peptide or PBS or they remained untreated. The activity accumulation of  $^{64}\text{Cu}$ -OVA-Th1 cells in the pulmonary LNs ( $6.8 \pm 1.1 \%ID/\text{cm}^3$ ) 24 h after injection was highest in the OVA-immunized and OVA-challenged animals and lowest in the untreated littermates ( $3.7 \pm 0.4 \%ID/\text{cm}^3$ ; Fig. 4A, left; Fig. 4B, upper). As expected,  $^{64}\text{Cu}$ -OVA-Th1 cells also accumulated significantly in the pulmonary LNs of nonimmunized OVA-challenged animals ( $6.1 \pm 0.5 \%ID/\text{cm}^3$ ), whereas in PBS-challenged animals, the activity values ( $4.6 \pm 0.5 \%ID/\text{cm}^3$ ) 24 h after T-cell transfer were similar to the back-

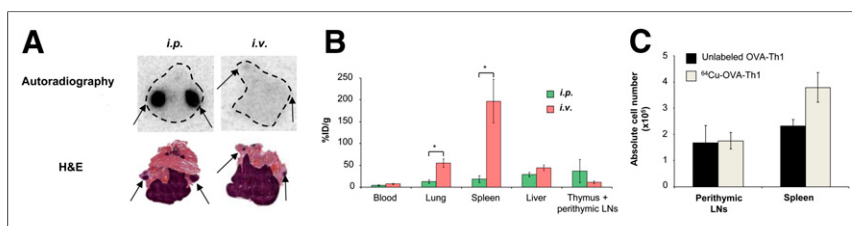


**FIGURE 3.**  $^{64}\text{Cu}$ -PTSM labeling does not impair in vivo OVA-Th1 cell homing. (A) Representative hematoxylin and eosin (H&E)-stained sections and autoradiography images of thymus and perithymic LNs 24 h after intravenous or intraperitoneal  $^{64}\text{Cu}$ -OVA-Th1 cell transfer. Autoradiography images revealed perithymic LNs (arrows) to be one of the early homing sites of  $^{64}\text{Cu}$ -OVA-Th1 cells after intraperitoneal transfer but not after intravenous administration ( $n = 3$ ). (B) Biodistribution analysis ( $\%ID/g$ ) of blood, lung, spleen, liver, and thymus (including perithymic LNs) was performed 40 h after intraperitoneal or intravenous  $^{64}\text{Cu}$ -OVA-Th1 cell transfer to confirm in vivo PET imaging results; 2-sampled Student  $t$  test.  $*P < 0.05$ . Mean  $\pm$  SEM ( $n = 6$ ). (C) FACS analysis of intraperitoneally administered nonlabeled or  $^{64}\text{Cu}$ -PTSM-labeled OVA-Th1 cells revealed almost equivalent numbers of nonlabeled and  $^{64}\text{Cu}$ -OVA-Th1 cells within perithymic LNs and increased number of  $^{64}\text{Cu}$ -OVA-Th1 cells in spleen. Mean  $\pm$  SEM ( $n = 4$ ). i.p. = intraperitoneal; i.v. = intravenous.

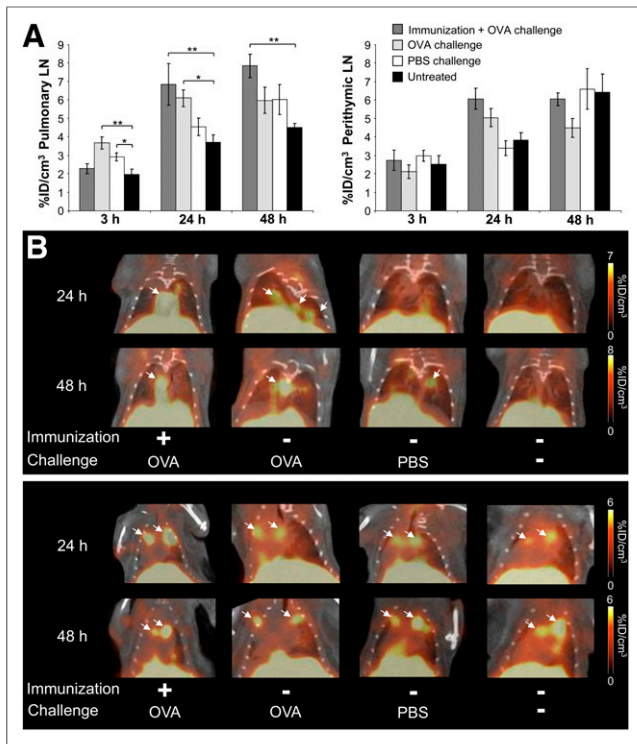


**FIGURE 4.**  $^{64}\text{Cu}$ -PTSM-labeled OVA-Th1 cells home specifically in draining lymphatic tissue at sites of OVA-induced AHR. (A) PET/CT measurements of activity accumulation of  $^{64}\text{Cu}$ -PTSM-labeled OVA-Th1 cells (%ID/cm<sup>2</sup>) in pulmonary LNs (left) and perithymic LNs (right) after intraperitoneal transfer of  $10^7$   $^{64}\text{Cu}$ -OVA-Th1 cells into diseased and control mice. Enhanced homing of OVA-Th1 cells in OVA-immunized and OVA-challenged mice to pulmonary LNs; Dunnett's test. \* $P < 0.05$ . \*\* $P < 0.01$ . Untreated,  $n = 6$ ; OVA-immunized + OVA-challenged,  $n = 7$ –19; OVA-challenged,  $n = 7$ –18; and PBS-challenged mice,  $n = 4$ –12. Mean  $\pm$  SEM. (B) Representative PET/CT images 24 and 48 h after intraperitoneal administration of  $^{64}\text{Cu}$ -OVA-Th1 cells focusing on pulmonary LNs (upper) and perithymic LNs (lower; arrows).

ground of untreated mice. The OVA-specific homing of  $^{64}\text{Cu}$ -OVA-Th1 cells in nonprimed but OVA-challenged mice was expected, because the peptide is absorbed and presented in the draining LNs. Specific accumulation in the pulmonary LNs persisted for 48 h only in the OVA-challenged mice that were immunized. These data suggest that the primed mice develop sustained inflammation in the lung. As observed in the lung and the pulmonary LNs, we detected a tendency toward increased OVA-specific accumulation of  $^{64}\text{Cu}$ -OVA-Th1 cells in the perithymic LNs of OVA-immunized and OVA-challenged mice 24 h after T-cell administration (Fig. 4A, right; Fig. 4B, lower), a point in time with most severe lung inflammation. Although the perithymic LNs are not the draining LNs of the lungs, they may be affected by the lung inflammation.

To exclude an unspecific signal caused by the  $^{64}\text{Cu}$  efflux from  $^{64}\text{Cu}$ -OVA-Th1 cells, we intraperitoneally injected 0.7 MBq of  $^{64}\text{Cu}$ -PTSM in OVA-immunized and OVA-challenged mice or in healthy PBS-challenged control mice. We could not identify unspecific  $^{64}\text{Cu}$ -PTSM accumulation in both experimental groups in the lung tissue, pulmonary, and perithymic LNs 24 and 48 h after injection (Fig. 5). The PET/CT measurements agreed with the autoradiography and biodistribution in the lung tissue and the thymus (Fig. 6; supplemental data).

## DISCUSSION

T-cell-based immunotherapy of cancer is an emerging novel therapeutic approach (18,19). Some data suggest that the adoptive transfer of autologous tumor-infiltrating lymphocytes may induce cancer regression in up to 50% of metastatic melanomas (20). Thus, tumor-associated antigen (TAA)-specific IFN- $\gamma$ -producing CD8<sup>+</sup> (Tc1) and CD4<sup>+</sup> T cells (Th1) display strong antitumor effects in humans and mice (19,21–23).

To gain deeper insights into the early homing patterns, to quantify T-cell accumulation at the homing sites, and to identify the best mode of TAA T-cell administration, we applied  $^{64}\text{Cu}$ -PTSM labeling and highly sensitive noninvasive in vivo PET imaging.  $^{64}\text{Cu}$ -PTSM labeling of T cells may be superior to other labeling strategies, and the transfer of this strategy from rodents to humans may be safe because no viral-based manipulation with reporter genes is required. Alternatively, Matsui et al. investigated a labeling strategy based on T-cell-specific radiolabeled antibodies, which were used for the in vivo labeling of the TAA T cells (6). Their data raise several concerns, because nonbound or nonspecifically bound radiolabeled antibodies produce a severe background signal (6). Furthermore, the antibody can cause immune reactions, and most importantly, specific antibody binding to T cells may depend on the delivery efficacy of the antibody in vivo to the sites of T-cell accumulation (6,24). Thus, the spatial and temporal T-cell detection and quantification would depend on the bioavailability and the pharmacokinetics of the antibody (24,25). Similar limitations apply for transduced cells that use a reporter probe (9).

Several research groups routinely use  $^{111}\text{In}$ -oxine, which is a SPECT tracer, for immune cell labeling, to reveal non-identified sites of inflammation in patients or to study cell trafficking in rodents (26,27). However, we detected with 0.7 MBq of  $^{111}\text{In}$ -oxine-labeled murine OVA-Th1 cells an induction of double-strand breaks (unpublished results), which even was more severe than with  $^{64}\text{Cu}$ . Furthermore, the detection sensitivity of SPECT is 100- to 1,000-fold lower than that of PET (13,28).

As an alternative to nuclear methods, MR imaging has been established preclinically and clinically. Several groups are focusing on T-cell-trafficking studies using SPIOs or  $^{19}\text{F}$ -labeled cells and  $^{19}\text{F}$  MR imaging (5,29–33). T cells labeled with SPIOs provide a negative contrast signal in MR images, from which it is challenging to extract information about the whole-body biodistribution of the labeled immune cells (5,30,31). The detection of individual homing sites without a priori knowledge and absolute quantification are impossible. Therefore, Thu et al. injected SPIO-labeled

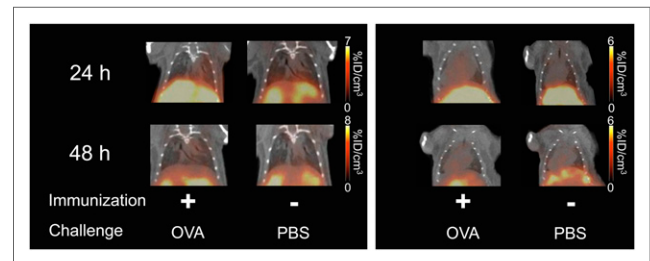


**FIGURE 5.** Distribution of  $^{64}\text{Cu}$ -PTSM in lung and perithymic LNs after intraperitoneal injection into OVA AHR-diseased and control mice. Representative PET/CT images 24 and 48 h after intraperitoneal administration of 0.7 MBq of  $^{64}\text{Cu}$ -PTSM indicate no accumulation of  $^{64}\text{Cu}$ -PTSM in lung tissue, pulmonary (left), and perithymic LNs (right). High-resolution template CT scan provided detailed anatomic information for accurate localization of  $^{64}\text{Cu}$ -PTSM. Scans were normalized to injected activity of  $10^7$   $^{64}\text{Cu}$ -OVA-Th1 cells in OVA AHR-diseased animals (Fig. 4).

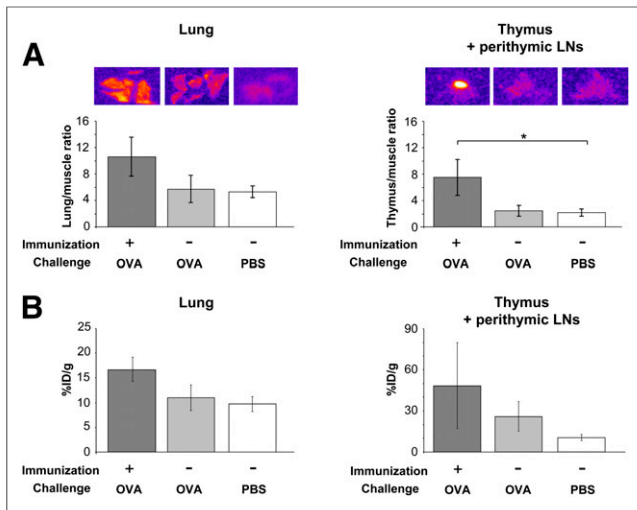


**FIGURE 6.**  $^{64}\text{Cu}$ -PTSM-labeled OVA-Th1 cells home specifically to lung and perithymic LNs of OVA AHR-diseased mice. (A) Autoradiography revealed 24 h after intraperitoneal  $^{64}\text{Cu}$ -OVA-Th1 cell administration increased lung-to-muscle and thymus-to-muscle ratios in OVA-immunized and OVA-challenged animals ( $n = 3$ ), compared with ratios in OVA-challenged ( $n = 5$ ) or PBS-challenged animals ( $n = 6$ ). Dunnett's test.  $*P < 0.05$ ; mean  $\pm$  SEM. (B) Biodistribution, performed 48 h after intraperitoneal  $^{64}\text{Cu}$ -OVA-Th1 cell injection, showed higher percentage injected dose per gram (%ID/g) in lung and thymus including perithymic LNs in OVA-immunized and OVA-challenged animals ( $n = 7$ ), compared with OVA- ( $n = 6$ ) or PBS-challenged animals ( $n = 5$ ); mean  $\pm$  SEM.

bone marrow stromal cells intracranially at a defined detection site for MR imaging (5). This is in sharp contrast to our approach, in which we injected the radiolabeled cells systemically and followed up and quantified their whole-body biodistribution *in vivo*. The  $^{19}\text{F}$  MR imaging approach is interesting but suffers from the low detection sensitivity of MR imaging, resulting in a measurement time of several hours even for larger cell clusters of tens of thousands of cells and a limited field of view (29,32,33).

Because direct radioactive labeling approaches for cells of interest are limited by the radionuclide half-life, the induction of double-strand breaks, and the dilution of the radiolabel due to cell proliferation, indirect labeling approaches using reporter genes are an alternative labeling strategy for long-term cell-tracking studies (34). We transduced OVA-Th1 cells with the triple-fusion cassette containing the herpes simplex thymidine kinase as PET reporter gene (7) but achieved only an insufficient transduction efficiency (unpublished results). In addition, the application of virally modified cells in humans raises ethical concerns (4).

Our study provides the first, to our knowledge, comprehensive evaluation of  $^{64}\text{Cu}$ -PTSM labeling of murine antigen-specific Th1 cells and the intracellular  $^{64}\text{Cu}$  accumulation and impact on viability, function, and double-strand breaks.

Thus far, only a few research groups have focused on  $^{64}\text{Cu}$ -PTSM labeling of cells for cell-tracking studies, and only 2 groups investigated the cellular  $^{64}\text{Cu}$  efflux of  $^{64}\text{Cu}$ -PTSM-labeled cells (8,14). In our studies, we characterized and quantified the efflux of  $^{64}\text{Cu}$  from murine OVA-Th1 cells *in vitro* for the first time in detail and detected in *in vitro* experiments an efflux of 53% within 5 h and 86% within 24 h after labeling with 0.7 MBq of  $^{64}\text{Cu}$ -PTSM. These *in vitro* experiments reflect, compared with *in vivo* conditions, a worst case because the cells are densely packed and thus exposed to extended radiation from neighboring cells and activity in the

medium. Adonai et al. performed efflux studies with C6 rat glioma cells and detected an efflux of 62% within 5 h and 78% within 24 h after the labeling procedure (8). Prince et al. claimed an efflux of 20% from human dendritic cells within the first hour after  $^{64}\text{Cu}$ -PTSM labeling but did not provide detailed efflux studies nor report the efflux 24 h after labeling (14). Thus, no direct comparison to our  $^{64}\text{Cu}$  efflux studies is possible because of the differences in cell type.

Th1 cells labeled with 0.7 MBq of  $^{64}\text{Cu}$  displayed only a slight reduction in viability, IFN- $\gamma$  secretion, and cell proliferation and an induction of phosphorylated  $\gamma$ -H2AX histones. In contrast to Adonai et al., who proposed the hypothesis that  $^{64}\text{Cu}$  is mainly retained in the cytoplasm, we also found  $^{64}\text{Cu}$  in the cell nucleus by EDX analysis. The double-strand breaks might be caused by the localized radiation within the nucleus because  $^{64}\text{Cu}$  decays in 18% by positron emission ( $\beta^+$ ) and in 40% by electron capture, emitting Auger electrons that are radiotoxic to DNA (35,36).

Most importantly, despite the impact of the radiolabel on OVA-Th1 cells, we detected almost equivalent numbers of intraperitoneally injected  $^{64}\text{Cu}$ -OVA-Th1 cells and nonlabeled OVA-Th1 cells in the perithymic LNs and spleens of littermates by FACS. This finding supports our hypothesis that the radiolabeling of Th1 cells causes only minor cell damage *in vivo*. In our *in vitro* conditions, the effect on viability and function was most likely overestimated and represents the worst-case scenario regarding radiolabeling/cell concentrations. Using  $^{64}\text{Cu}$ -PTSM labeling of OVA-Th1 cells, we were able to identify clear differences between the intraperitoneal and intravenous administration of Th1 cells and were able to detect OVA-Th1 cells within a single LN for up to 40 h. Moreover, we could follow specific OVA-Th1 cell-trafficking to the site of inflammation in an experimental model of OVA-induced lung inflammation for up to 48 h. No  $^{64}\text{Cu}$  accumulation in the pulmonary and perithymic LNs could be observed in mice with OVA AHR after intraperitoneal injection of free  $^{64}\text{Cu}$ -PTSM (Fig. 5). Thus,  $^{64}\text{Cu}$ -PTSM labeling and PET imaging of autologous leukocytes is an appropriate approach to track immune cells *in vivo* and permits the study of the mechanistic properties of cell homing and function. The temporal monitoring also revealed the important finding that all trafficking processes occur quickly, most within several minutes or hours, suggesting that a fast imaging modality, such as PET, is beneficial. Interestingly, we also found that Th1 cells accumulated in the perithymic LNs, which was described so far in only one other report and leaves the underlying mechanism open to question (37). In contrast to Klinkert, we observed accumulation in perithymic LNs after intraperitoneal but not after intravenous injection, and PET imaging revealed that most of the Th1 cells had already reached the perithymic LNs 2 h after injection. Because the role of perithymic LNs remains unclear, further studies using different cell populations and stimulations are necessary.

Although PET exhibits in general a good quantification accuracy, specifically compared with other imaging modalities, it clearly reveals limitations in absolute quantification in small organs such as LN or the spleen; however, it still allows comparative and temporal quantification. There are large differences between *ex vivo*  $\gamma$  counting and *in vivo* PET quantification of the spleen (Fig. 2A) and lung. The density of the lung is low, overestimating the weight of the lung in the PET analysis ( $1 \text{ cm}^3 \neq 1 \text{ g}$ ). The discrepancy of the quantification of the spleen is caused by a large volume of interest drawn on normalized PET images not corresponding to the long but flat shape of the spleen. This significant quantification difference is specifically reflected in spleens of intravenously injected mice that have, compared with spleens of intraperitoneally injected animals, a much

higher signal leading to larger volumes of interest. In addition, the tiny spleen of a mouse yields a large partial-volume effect and low recovery (38). Thus, the in vivo quantification accuracy in such studies would significantly improve using combined PET/MR, yielding high resolution morphology and soft-tissue contrast, for an accurate placement of volumes of interest (1).

## CONCLUSION

For a better understanding of the basic mode of T-cell homing and for the improvement of established T-cell-based treatment protocols, a knowledge of the homing dynamics of adoptively transferred T cells is essential and can be gained using PET imaging of <sup>64</sup>Cu-PTSM-labeled cells. <sup>64</sup>Cu-PTSM labeling of T cells can thus provide insights into the homing dynamics of TAA-specific T cells and into the effector phase of autoimmune diseases. The high-detection sensitivity of PET permits the labeling of only a small fraction of the cells in therapeutic interventions to monitor the trafficking routes in vivo without impairing the long-term functionality of most of the administered therapeutic cells. The established methods are therefore valuable for personalized medicine strategies.

## DISCLOSURE

The costs of publication of this article were defrayed in part by the payment of page charges. Therefore, and solely to indicate this fact, this article is hereby marked "advertisement" in accordance with 18 USC section 1734. This work was supported by the SFB685 and NIH R03 grants. The Department of Preclinical Imaging and Radiopharmacy serves as Reference and Training site for Siemens. Only institutional but no personal funds are related to this. No other potential conflict of interest relevant to this article was reported.

## ACKNOWLEDGMENTS

We thank Nadine Bauer, Maren Koenig, Renate Nordin, and Denis Lamparter for excellent technical support.

## REFERENCES

- Judenhofer MS, Wehrl HF, Newport DF, et al. Simultaneous PET-MRI: a new approach for functional and morphological imaging. *Nat Med*. 2008;14:459–465.
- Cherry SR. Fundamentals of positron emission tomography and applications in preclinical drug development. *J Clin Pharmacol*. 2001;41:482–491.
- Constantinescu CC, Mukherjee J. Performance evaluation of an Inveon PET preclinical scanner. *Phys Med Biol*. 2009;54:2885–2899.
- Yaghoubi SS, Creusot RJ, Ray P, Fathman CG, Gambhir SS. Multimodality imaging of T-cell hybridoma trafficking in collagen-induced arthritic mice: image-based estimation of the number of cells accumulating in mouse paws. *J Biomed Opt*. 2007;12:064025.
- Thu MS, Bryant LH, Coppola T, et al. Self-assembling nanocomplexes by combining ferumoxytol, heparin and protamine for cell tracking by magnetic resonance imaging. *Nat Med*. 2012;18:463–467.
- Matsui K, Wang Z, McCarthy TJ, Allen PM, Reichert DE. Quantitation and visualization of tumor-specific T cells in the secondary lymphoid organs during and after tumor elimination by PET. *Nucl Med Biol*. 2004;31:1021–1031.
- Ray P, Tsien R, Gambhir SS. Construction and validation of improved triple fusion reporter gene vectors for molecular imaging of living subjects. *Cancer Res*. 2007;67:3085–3093.
- Adonai N, Nguyen KN, Walsh J, et al. Ex vivo cell labeling with <sup>64</sup>Cu-pyruvaldehyde-bis(N4-methylthiosemicarbazone) for imaging cell trafficking in mice with positron-emission tomography. *Proc Natl Acad Sci USA*. 2002;99:3030–3035.
- Nair-Gill ED, Shu CJ, Radu CG, Witte ON. Non-invasive imaging of adaptive immunity using positron emission tomography. *Immunol Rev*. 2008;221:214–228.
- Blower PJ, Lewis JS, Zweit J. Copper radionuclides and radiopharmaceuticals in nuclear medicine. *Nucl Med Biol*. 1996;23:957–980.
- Biesemeier A, Schraermeyer U, Eibl O. Quantitative chemical analysis of ocular melanosomes in stained and non-stained tissues. *Micron*. 2011;42:461–470.
- Eibl O, Schultheiss S, Blitgen-Heinecke P, Schraermeyer U. Quantitative chemical analysis of ocular melanosomes in the TEM. *Micron*. 2006;37:262–276.
- Parente-Pereira AC, Burnet J, Ellison D, et al. Trafficking of CAR-engineered human T cells following regional or systemic adoptive transfer in SCID beige mice. *J Clin Immunol*. 2011;31:710–718.
- Prince HM, Wall DM, Ritchie D, et al. In vivo tracking of dendritic cells in patients with multiple myeloma. *J Immunother*. 2008;31:166–179.
- Torjman MC, Joseph JI, Munsick C, Morishita M, Grunwald Z. Effects of isoflurane on gastrointestinal motility after brief exposure in rats. *Int J Pharm*. 2005;294:65–71.
- Fuchs K, Kukuk D, Mahling M, et al. Impact of anesthetics on 3'-[<sup>18</sup>F]fluoro-3'-deoxythymidine ([<sup>18</sup>F]FLT) uptake in animal models of cancer and inflammation. *J Mol Imaging*. 2013;12:277–287.
- Schopf A, Heilmann A, Boue L, Mossman H, Brocker T, Rocken M. Th2 cells shape the differentiation of developing T cell responses during interactions with dendritic cells in vivo. *Eur J Immunol*. 2003;33:1697–1706.
- Ziegler A, Heidenreich R, Braumüller H, et al. EpCAM, a human tumor-associated antigen promotes Th2 development and tumor immune evasion. *Blood*. 2009;113:3494–3502.
- Müller-Hermelink N, Braumüller H, Pichler B, et al. TNFR1 signaling and IFN-gamma signaling determine whether T cells induce tumor dormancy or promote metastatic carcinogenesis. *Cancer Cell*. 2008;13:507–518.
- Besser MJ, Shapira-Frommer R, Treves AJ, et al. Clinical responses in a phase II study using adoptive transfer of short-term cultured tumor infiltration lymphocytes in metastatic melanoma patients. *Clin Cancer Res*. 2010;16:2646–2655.
- Rosenberg SA. Cell transfer immunotherapy for metastatic solid cancer—what clinicians need to know. *Nat Rev Clin Oncol*. 2011;8:577–585.
- Restifo NP, Dudley ME, Rosenberg SA. Adoptive immunotherapy for cancer: harnessing the T cell response. *Nat Rev Immunol*. 2012;12:269–281.
- Braumüller H, Wieder T, Brenner E, et al. T-helper-1-cell cytokines drive cancer into senescence. *Nature*. 2013;494:361–365.
- Wu AM, Senter PD. Arming antibodies: prospects and challenges for immunconjugates. *Nat Biotechnol*. 2005;23:1137–1146.
- Alt K, Wiehr S, Ehrlichmann W, et al. High-resolution animal PET imaging of prostate cancer xenografts with three different <sup>64</sup>Cu-labeled antibodies against native cell-adherent PSMA. *Prostate*. 2010;70:1413–1421.
- Djekidel M, Brown RK, Pietsch M. Benefits of hybrid SPECT/CT for <sup>111</sup>In-oxine- and Tc-99m-hexamethylpropylene amine oxime-labeled leukocyte imaging. *Clin Nucl Med*. 2011;36:e50–e56.
- Roca M, de Vries EF, Jamar F, Israel O, Signore A. Guidelines for the labelling of leucocytes with <sup>111</sup>In-oxine: Inflammation/Infection Taskgroup of the European Association of Nuclear Medicine. *Eur J Nucl Med Mol Imaging*. 2010;37:835–841.
- Gildehaus FJ, Haasters F, Drosse I, et al. Impact of indium-111 oxine labelling on viability of human mesenchymal stem cells in vitro, and 3D cell-tracking using SPECT/CT in vivo. *Mol Imaging Biol*. 2011;13:1204–1214.
- Srinivas M, Heerschap A, Ahrens ET, Figdor CG, de Vries IJ. <sup>19</sup>F MRI for quantitative in vivo cell tracking. *Trends Biotechnol*. 2010;28:363–370.
- Halin C, Mora JR, Sumen C, von Andrian UH. In vivo imaging of lymphocyte trafficking. *Annu Rev Cell Dev Biol*. 2005;21:581–603.
- Kircher MF, Allport JR, Graves EE, et al. In vivo high resolution three-dimensional imaging of antigen-specific cytotoxic T-lymphocyte trafficking to tumors. *Cancer Res*. 2003;63:6838–6846.
- Ahrens ET, Flores R, Xu H, Morel PA. In vivo imaging platform for tracking immunotherapeutic cells. *Nat Biotechnol*. 2005;23:983–987.
- Srinivas M, Turner MS, Janjic JM, Morel PA, Laidlaw DH, Ahrens ET. In vivo cytometry of antigen-specific T cells using <sup>19</sup>F MRI. *Magn Reson Med*. 2009;62:747–753.
- Kircher MF, Gambhir SS, Grimm J. Noninvasive cell-tracking methods. *Nat Rev Clin Oncol*. 2011;8:677–688.
- Adelstein SJ, Merrill C. Sosman Lecture. The Auger process: a therapeutic promise? *AJR*. 1993;160:707–713.
- Lewis J, Laforest R, Buettner T, et al. Copper-64 diacetyl-bis(N4-methylthiosemicarbazone): an agent for radiotherapy. *Proc Natl Acad Sci USA*. 2001;98:1206–1211.
- Klinkert WE. Homing of antigen-specific T cells in the Lewis rat. I. Accumulation of antigen-reactive cells in the perithymic lymph nodes. *J Immunol*. 1987;139:1030–1036.
- Mannheim JG, Judenhofer MS, Schmid A, et al. Quantification accuracy and partial volume effect in dependence of the attenuation correction of a state-of-the-art small animal PET scanner. *Phys Med Biol*. 2012;57:3981–3993.